RAA 2020 Vol. **20** No. **12**, 193(16pp) doi: 10.1088/1674-4527/20/12/193

http://www.raa-journal.org *http://iopscience.iop.org/raa*

***R**esearch in*
***A**stronomy and*
***A**strophysics*

Parametric resonance orbit analysis for irregular shaped asteroids based on the perturbed particle-linkage model

Ying-Jing Qian (钱霙婧), Zhen Si (司震), Xiao-Dong Yang (杨晓东) and Wei Zhang (张伟)

Beijing Key Laboratory of Nonlinear Vibrations and Strength of Mechanical Structures, College of Mechanical Engineering, Beijing University of Technology, Beijing 100124, China; *candiceqyj@163.com*

Received 2020 March 21; accepted 2020 June 9

Abstract There are plentiful asteroids moving periodically around their central primaries, such as the Sun. Due to the perturbation of the central primary, the gravitational force of the perturbed asteroid system varies periodically. In this paper, based on the idea of integrating the solar gravitational force as a part of the system instead of treating it as perturbation, the parametric resonance response is investigated. A novel type of stable parametric resonance orbits has been detected. It is found that the steady-state motion amplitude of parametric resonance orbit is determined by the frequency-response equation. The stability of the novel orbits has also been demonstrated. The new type of orbits may contribute to possible asteroid exploration missions.

Key words: asteroids: general — space vehicles — celestial mechanics

1 INTRODUCTION

Irregular asteroids are quite common in the solar system and extrasolar systems. It has been recognized that exploration missions to asteroids can provide key information in the study of the origin of our solar system, the evolution of planets and human beings. Some well-known missions include NEAR Shoemaker which orbited Eros (Prockter et al. 2002), the extension mission of Chang'e-2 which made a flyby to Toutatis (Huang et al. 2013), Hayabusa which landed on Itokawa (Nardi et al. 2019), and OSIRIS-Rex which successfully orbited Bennu (Lauretta et al. 2019). Particularly, the stable periodic orbits in design have drawn great attention (Jiang et al. 2017; Liu et al. 2012; Zeng & Alfriend 2017). The investigation of periodic orbits yields essential information when a non-integrable dynamical system is treated (Jiang et al. 2015c).

The dynamic environment for the irregular asteroid is perhaps the most strongly perturbed astrodynamics environment found in the solar system. The combination of familiar factors may propose new challenges, including strongly non-spherical body shapes, the arrangement of spin states and rates, gravitational perturbations and solar radiation pressures (Scheeres 2012; Jiang & Baoyin 2016; Li et al. 2018). Consequently, the problem of stable periodic orbits for irregular asteroids is more challenging compared to planets.

A lot of work has been devoted to the mechanical explanation of stable periodic orbits, by both analytical and numerical methods. The analytic framework of all this work is usually the classical three-body problem in the planar (both elliptic and circular) cases in the asteroid's body-fixed frame based on the simplified segment model (Eros & Elipe 2004; Bartczak & Breiter 2003) and dipole model (Zeng & Alfriend 2017; Zeng et al. 2016, 2018). Analytical periodic orbits can be obtained in the vicinity of the asteroids' libration points or about the asteroids. The numerical integration method has been used to ensure the accuracy by forcing the end-points of an orbit to coincide with the start-point. If one periodic orbit is located, other orbits from this family may be found via the continuation method by varying some parameters, such as Jacobi constant or orbit period. Scheeres et al. (1996) found some families of periodic orbits around 4769 Castalia, using a gravitational model of a polyhedron. The periodic orbit, in resonance conditions, has been studied by Scheeres et al. (2000). Shi et al. (2019) apply the numerical method to the binary asteroid (66391) 1999 KW4 to solve the periodic orbits in the vicinity. Recently, the hierarchical grid searching method was proposed by

Yu & Baoyin (2012) which can be used to find periodic orbits. Jiang et al. (2017) found five different types of stable periodic orbits around minor celestial bodies, using the topological classifications of periodic orbits and the grid search method. This method makes the global search for 3D periodic orbits around irregular bodies possible.

The aforementioned works have shown the complexity and variety of periodic orbits in irregular gravitational fields, which are definitely beneficial to the understanding of close proximity dynamics. It is noticed that most studies focus on computing specific periodic families around the asteroid's or system's equilibrium points (Jiang et al. 2015a; Bellerose & Scheeres 2007; Shi et al. 2018), their stability properties (Chanut et al. 2014; Wang & Xu 2014; Wang & Xu 2013), bifurcation characteristic (Jiang et al. 2015b), and the existence of inherent relationship between these periodic families (Hou et al. 2018) only with consideration of the central gravitational attraction and the non-spherical gravitation. Other studies focus on how the orbital secular dynamics will evolve over time due to the non-spherical gravitation (Lei et al. 2019) and solar radiation pressures (Feng & Hou 2019).

However, if the spacecraft is not sufficiently near the surface of an irregular asteroid, the solar gravitation and pressure to the particle has to be considered, which can be found in Scheeres (2012). It is known that the solar radiation pressure behaves as external excitations, in which the excitations appear as inhomogeneities in the governing differential equations (Feng & Hou 2019). However, the solar gravitational perturbation excitations always appear as coefficients in the governing differential equations (terms include x and y). Such terms lead to differential equations with time-varying coefficients, just like the famous Hill equation and Mathieu equation. These excitations are called parametric excitations. Moreover, in contrast with the case of solar radiation pressure external excitations in which a small excitation cannot produce a large response unless the frequency of the excitation is close to one of the natural frequencies of the system, a small solar gravitational perturbation parametric excitation can produce a large response when the frequency of the excitation is close to twice of the natural frequencies of the system. Generally, those two kinds of resonance cannot happen at the same time (Nayfeh & Mook 1995).

In this study, we focus on the parametric excitations caused by solar gravitational perturbation. Innovated by this point, an interesting question arises: with the solar gravity, under what conditions a spacecraft will be able to stay bound to an asteroid in the presence of these additional forces? Can we utilize the solar gravitation force to generate stable periodic orbits instead of overcoming the solar gravitation force as perturbation? The answer is yes. According to the nonlinear oscillation theory (Nayfeh & Mook 1995), there exist stable periodic orbits caused by parametric resonance.

As is well known, if a parametric excitation system is truly linear, the amplitude grows boundlessly when the parametric resonance occurs. A confirmatory and observable experiment conducted by Mandelstam (1934) showed that the amplitude of a specially designed linear oscillation circuit grew until the insulation was destroyed by an excessive voltage. The parametric resonance conditions can be obtained analytically by the perturbation technique. Representative works can be found in Alfriend & Rand (1968) who studied the resonance conditions for infinitesimal motions in the non-autonomous elliptic restricted three-body problem. Similarly, the conditions for the principal parametric resonance are obtained analytically by Qian et al. (2018a) for the non-autonomous bicircular four-body problem. The linear theory is useful in determining the initial growth or decay, which can be used in finding the parametric resonance condition. It becomes inadequate if the system possesses any nonlinearity and cannot be used to find stable periodic orbits for trajectory design.

The nonlinearity cannot be neglected in the engineering field, which comes into play as soon as the amplitude of the motion becomes higher. The nonlinear effect appears with a growing amplitude, resulting in limit cycles. One example is the specially designed nonlinear oscillation circuit by Mandelstam (1934). Similarly, Hsu (1974) determined analytical solutions in Jacobi elliptic function for a nonlinear Hill equation. Strong nonlinearities may lead to other non-periodic responses (Jafari Nadoushan & Assadian 2015).

Thus, based on the idea of utilizing the solar gravitational force as part of the system instead of treating it as perturbations, the concept of parametric resonance from nonlinear oscillation theory is adopted in this study to design the stable parametric resonance orbits for asteroids. In order to consider the non-spherical gravitation and solar gradational force, a perturbed particle-linkage model is used.

This study expands a set of existing periodic orbits for asteroid systems. The contributions of this study can be summarized as: (1) the boundary of the region where the parametric resonance periodic orbit can exist is shown; (2) the amplitude of the steady-state is determined by a frequency-response equation; and (3) the stable steady-state solution for parametric resonance orbits are found.

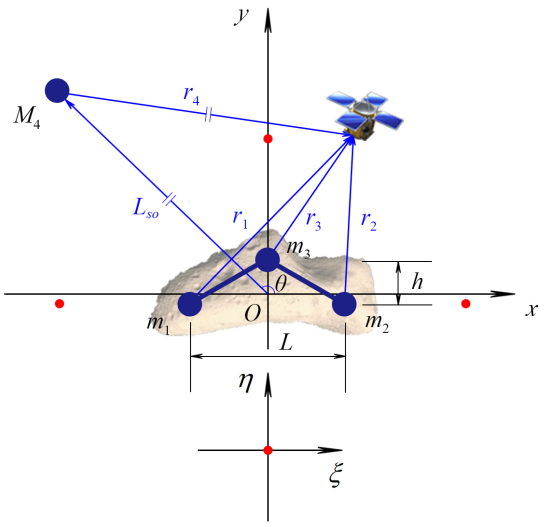

Fig. 1 Perturbed particle-linkage model.

The structure of this paper is as follows. First, the perturbed particle-linkage model is described in Section 2. In Section 3, the region in which the parametric resonance can exist is computed analytically. In Section 4, the method of multiple scales is used to obtain a stable steady-state solution for parametric resonance orbits. Furthermore, illustrative numerical simulations are performed to demonstrate the proposed orbits in Section 5. The paper ends with the conclusions in Section 6.

2 DYNAMICAL MODEL

Since parametric excitations caused by solar gravitational perturbation are focused, a perturbed particle-linkage model is enough to model the gravity caused by the irregular minor celestial bodies.

The perturbed particle-linkage model is composed of three primaries m_1, m_2 and m_3, separated by two massless rods, and their barycenter is moving in a circular orbit around a large body M_4. All bodies move in a plane. The distance from M_4 to the asteroid is much greater than the distances between every two primaries inside the asteroid. The total system mass of the asteroid is M where $M = m_1 + m_2 + m_3$. It is assumed that $m_3 \geq m_1 = m_2$, and the three primaries are formed as an isosceles triangle configuration. The distance between m_2 and m_3 is defined as L, and the distance from m_3 to the rod connecting m_2 and m_3 is h.

A schematic map of this system is conveniently described in the asteroid's body-fixed coordinate system $(O - xyz)$, centered at the mass center of the asteroid shown in Figure 1. The axis O_z is aligned with the angular velocity of the asteroid Ω, axis O_x is parallel to the line connecting the two primaries pointing from m_1 to m_2, and axis O_y is determined by the right-handed frame. The massless spacecraft moves under the gravitational attractions of all primaries in this system, but the motions of the primaries are assumed to be not affected by the spacecraft.

The non-dimensionalization is applied in the following study, such that the length unit is the distance L between m_1 and m_2, the time unit is Ω^{-1} and the mass unit is M. We introduce $\mu = m_1/M$ as the mass parameter of the system, then the dimensional masses for m_1, m_2, m_3 and M_4 can be expressed as

$$\mu_1 = \mu, \quad \mu_2 = \mu, \quad \mu_3 = \frac{m_3}{M} = 1 - 2\mu, \quad \mu_s = \frac{M_4}{M}. \tag{1}$$

Further, we introduce the length ratio $\sigma = h/L$. The σ is positive when m_3 is above the mass center of the asteroid, and is negative alternatively. The positions of three primaries can be written as $(-0.5, -(1 - 2\mu)\sigma)$, $(0.5, -(1 - 2\mu)\sigma)$, $(0, 2\mu\sigma)$, respectively. Since the barycenter of the asteroid moves in a circular orbit around M_4 with constant distance L_{so}, the position of M_4 can be written as $(L_{so}\cos\theta, L_{so}\sin\theta)$ where θ is the counterclockwise measured angle between the x axis and the line connecting M_4 and asteroid's barycenter, O.

With the definition above, the equations governing the orbits of the spacecraft are obtained in $O - xy$ as:

$$\begin{aligned}
\ddot{x} - 2\dot{y} = x - & \\
& k\left(\sum_{i=1}^{3}\frac{\mu_i\,(x - x_i)}{r_i^3} + \frac{\mu_s}{r_4^3}\,(x - L_{so}\cos\theta) + \frac{\mu_s}{L_{so}^2}\cos\theta\right), \\
\ddot{y} + 2\dot{x} = y - & \\
& k\left(\sum_{i=1}^{3}\frac{\mu_i\,(y - y_i)}{r_i^3} + \frac{\mu_s}{r_4^3}\,(y - L_{so}\sin\theta) + \frac{\mu_s}{L_{so}^2}\sin\theta\right),
\end{aligned} \tag{2}$$

where k is the dimensionless parameter which represents the ratio between the gravitational force and the centrifugal force, and can be expressed as

$$k = \frac{GM}{\Omega^2 L^3}, \tag{3}$$

and r_1, r_2, r_3, r_4 are the distances from m_1, m_2, m_3, M_4 to the spacecraft, respectively.

Since spacecraft motion surrounds the asteroid, we can expand $1/r_4^3$ as follows,

$$\frac{1}{r_4^3} \approx L_{so}^{-3}\left[1 + 3\frac{(x\cos\theta + y\sin\theta)}{L_{so}}\right], \tag{4}$$

where $r = \sqrt{x^2 + y^2}$ is the distance from spacecraft to the barycenter O. Defining

$$\beta = \mu_s / L_{so}^3, \tag{5}$$

as the fourth body's characteristic parameter and omitting nonlinear excitation terms, the equation of motion Equation (2) can be further reduced to

$$\begin{aligned}\ddot{x}-2\dot{y} &= \left(1+\frac{1}{2}k\beta\right)x-\frac{k\mu\,(x-x_1)}{r_1^3}-\frac{k\mu\,(x-x_2)}{r_2^3}\\ &\quad-\frac{k(1-2\mu)\,(x-x_3)}{r_3^3}+\frac{3}{2}k\beta(x\cos 2\theta+y\sin 2\theta),\\ \ddot{y}+2\dot{x} &= \left(1+\frac{1}{2}k\beta\right)y-\frac{k\mu\,(y-y_1)}{r_1^3}-\frac{k\mu\,(y-y_2)}{r_2^3}\\ &\quad-\frac{k(1-2\mu)\,(y-y_3)}{r_3^3}+\frac{3}{2}k\beta(x\sin 2\theta-y\cos 2\theta).\end{aligned} \tag{6}$$

It is clear that M_4's gravitational force consists of two parts: the direct constant gravity part due to the average gravitational force that presents in the linear stiffness terms as $1/2k\beta x$ and $1/2k\beta y$, and the parametric excitation part due to the periodic variation of the fourth body's position. Correspondingly, we can divide the system into two parts, just like the famous *Mathieu equation*: the unperturbed system, which is expressed as

$$\ddot{x}-2\dot{y}=\frac{\partial V}{\partial x},\ddot{y}+2\dot{x}=\frac{\partial V}{\partial y}, \tag{7}$$

where effective potential V is written as

$$V=\left(1+\frac{1}{2}k\beta\right)\frac{x^2+y^2}{2}+k\left(\frac{\mu}{r_1}+\frac{\mu}{r_2}+\frac{(1-2\mu)}{r_3}\right), \tag{8}$$

and the parametric excitation part, which contains the terms with the non-autonomous sine and cosine functions. Note that, the unperturbed system is different from the classical particle-linkage model system. The system's stiffness terms are altered by the fourth body's characteristic parameter β in Equation (6) which will finally affect the natural frequencies of the system.

The equilibrium points (x_0, y_0) are relevant to the mass parameter μ, length ratio σ, the dimensionless parameter k, and the fourth body's characteristic parameter β. With given parameters μ, σ, k, β we can generate the zero-value contours of $V_x = \partial V/\partial x$ and $V_y = \partial V/\partial y$ in the $x-y$ plane, from which the positions of intersection points can be assumed. The Newton-Raphson method is adopted to calculate the accurate locations of equilibrium points (Lei & Xu 2015). When $\beta = 0$, the system recovers to the classical particle-linkage model. The values of μ, σ, k for a known asteroid can be computed by the method in Yang et al. (2018). With given μ, σ, k, β two examples are denoted as blue dots and shown in Figure 2. There are four outside equilibrium points for both examples.

In order to analyze the system's parametric resonance orbit in Equation (2), it is necessary to move the origin

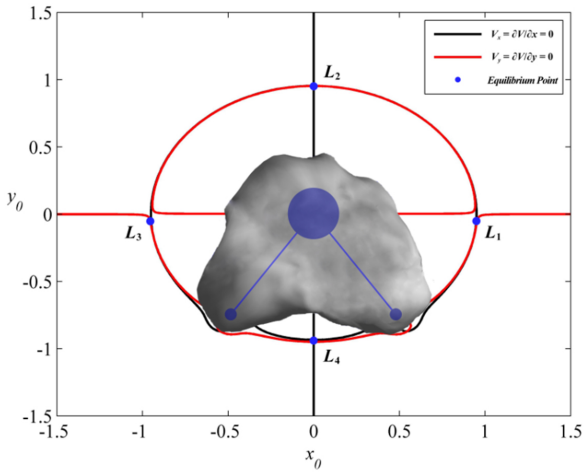

$\mu = 0.0019$, $\sigma = 0.8$, $k = 0.9$, $\beta = 0.1$

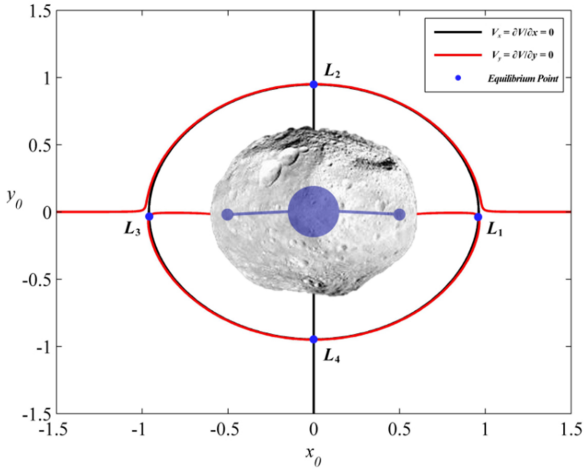

Vesta: $\mu = 0.01$, $\sigma = 0.0201$, $k = 0.8631$, $\beta = 0$

Fig. 2 Distributions of equilibrium points with variations of parameters

of the coordinate system from the mass center of the asteroid to its corresponding unperturbed system's stable equilibrium point. In addition, the unit of length is rescaled as the distance γ_0 between the equilibrium point and its closest primary (m_1, m_2 or m_3). In the following study, without loss of generality, we choose equilibrium point L_0 as a typical example. Note that, L_0 can be any stable point obtained in Section 2.2.

In the new coordinate system, named as $L_0-\xi\eta$, the directions of the ξ-, and η- are in parallel with those of the asteroid's body-fixed system, referred to Figure 1. The relationship between the $L_0-\xi\eta$ and $O-xy$ can be expressed as $(\xi,\eta)^T = (x-x_0, y-y_0)^T/\gamma_0$, where (x_0, y_0) are the position of corresponding stable equilibrium point in the asteroid's body-fixed system. Then, the term $1/r_i$ appearing in the effective potential V

in Equation (8) can be expanded as

$$\frac{1}{r_i} = \frac{1}{\gamma_0} \frac{1}{\sqrt{(\xi - E_i)^2 + (\eta - F_i)^2}}, i = 1, 2, 3 \quad (9)$$

Then, the linear part of Equation (6) can be rewritten as

$$\begin{aligned} \ddot{\xi} - 2\dot{\eta} - V^0_{\xi\xi}\xi - V^0_{\xi\eta}\eta &= E_0 + \frac{3}{2}k\beta\xi\cos 2\theta + \frac{3}{2}k\beta\eta\sin 2\theta, \\ \ddot{\eta} + 2\dot{\xi} - V^0_{\xi\eta}\xi - V^0_{\eta\eta}\eta &= F_0 + \frac{3}{2}k\beta\xi\sin 2\theta - \frac{3}{2}k\beta\eta\cos 2\theta, \end{aligned} \quad (10)$$

where

$$\begin{aligned} V^0_{\xi\xi} &= \left(1 + \frac{k\beta}{2}\right) + \sum_{i=1}^{3} \frac{\mu_i k \left(2E_i^2 - F_i^2\right)}{\gamma_0^3 D_i^5}, \\ V^0_{\eta\eta} &= \left(1 + \frac{k\beta}{2}\right) + \sum_{i=1}^{3} \frac{\mu_i k \left(2F_i^2 - E_i^2\right)}{\gamma_0^3 D_i^5}, \\ V^0_{\xi\eta} &= \sum_{i=1}^{3} \frac{3\mu_i k E_i F_i}{\gamma_0^3 D_i^5}, \quad E_i = \frac{x_i - x_0}{\gamma_0}, \\ F_i &= \frac{y_i - y_0}{\gamma_0}, \quad D_i^2 = E_i^2 + F_i^2, \\ E_0 &= \left(1 + \frac{\beta k}{2}\right)\frac{x_0}{\gamma_0} + \sum_{i=1}^{3} \frac{\mu_i k E_i}{\gamma_0^3 D_i^3}, \\ F_0 &= \left(1 + \frac{\beta k}{2}\right)\frac{y_0}{\gamma_0} + \sum_{i=1}^{3} \frac{\mu_i k F_i}{\gamma_0^3 D_i^3}. \end{aligned}$$

The partial derivatives of V are denoted by subscripts ξ or η. The superscript 0 indicates that the derivatives are to be evaluated at the equilibrium points. The over dots denote derivatives with respect to the actual time. Due to the symmetry of the system model in Figure 1, it is found that, for L_2 point and L_4 point, $D_1 = D_2$, $E_1 = -E_2$, $E_3 = 0$, $F_1 = F_2$ and $V^0_{\xi\eta} = 0$.

Note that, in Equation (10), such a system can be cast into an autonomous system under a small time-dependent perturbation by taking $3k\beta/2$ as the parametric excitation amplitude.

3 PARAMETRIC RESONANCE REGION

In the following study, we try to find the region in which the parametric resonance may exist. According to Nayfeh & Mook (1995), there are two important preconditions. Firstly, the analysis should be carried out in the vicinity of the stable equilibrium points to ensure the possible periodic solutions. Secondly, the parametric resonance occurs when the parametric frequency is close to the twice of the system's natural frequencies. Combining these two preconditions, the valid ranges of μ, σ, k, β for parametric resonance to occur can be found.

3.1 Precondition I: Stable Equilibrium Point

For the ξ-η components, the characteristic equation for the linear part of system in Equation (10) is

$$\lambda^4 + \left(4 - V^0_{\xi\xi} - V^0_{\eta\eta}\right)\lambda^2 + V^0_{\xi\xi}V^0_{\eta\eta} - \left(V^0_{\eta\xi}\right)^2 = 0. \quad (11)$$

The roots λ of the characteristic Equation (11) play a crucial role to determine the motions around equilibrium points. An equilibrium point will be stable if the above Equation (11) has pure imaginary roots or complex roots with negative real parts. This happens if the following conditions hold

$$\begin{cases} 4 - V^0_{\xi\xi} - V^0_{\eta\eta} > 0, \\ \left(V^0_{\xi\xi} + V^0_{\eta\eta} - 4\right)^2 - 4\left(V^0_{\xi\xi}V^0_{\eta\eta} - \left(V^0_{\xi\eta}\right)^2\right) > 0, \\ V^0_{\xi\xi}V^0_{\eta\eta} - \left(V^0_{\xi\eta}\right)^2 > 0, \end{cases} \quad (12)$$

which presents the valid ranges of μ, σ, k, β for the existence of stable equilibrium points. Examples are shown in Section 5.

3.2 Precondition II: Frequencies Relations

Based on Equation (11), the natural frequencies of the unperturbed particle-linkage model system around the L_0 are obtained as

$$i\omega_{1,2} = \sqrt{\frac{\left(4 - V^0_{\xi\xi} - V^0_{\eta\eta}\right) \mp \sqrt{\left(V^0_{\xi\xi} + V^0_{\eta\eta} - 4\right)^2 - 4\left(V^0_{\xi\xi}V^0_{\eta\eta} - \left(V^0_{\xi\eta}\right)^2\right)}}{2}}. \quad (13)$$

In addition, the frequency Ω_s for M_4 moving around the mass center of the asteroid is a two-body problem and satisfies Kepler's third law. In an inertial coordinate, that is

$$\Omega_s = \sqrt{\frac{\mu_s}{L_{so}^3}} = \sqrt{\beta}. \tag{14}$$

Since θ is the angle between the x axis and the line from the barycenter to M_4 in Figure 1, the frequency for θ rotating respect to the x axis in the asteroid's body-fixed coordinate system is

$$\omega = \sqrt{\frac{1}{k}} - \sqrt{\beta}. \tag{15}$$

In this way, θ in Equation (10) can be rewritten as $\theta = \omega t$.

Generally, for a two-dimensional system, there are two natural frequencies ω_1 and ω_2 (assuming that $\omega_2 > \omega_1$) denoting the long and the short period in orbit dynamics, respectively. Thus, two resonance types, named first and second principal resonances, are theoretically possible phenomena. As known, when μ, σ, k and β satisfy the exact resonance relations between the parametric frequency and the system's natural frequencies that $\omega = 2\omega_1$ or $\omega = 2\omega_2$, the whole system will definitely generate resonant responses. Even the values of μ, σ, k and β are close to the resonance relations, the system may present resonant responses (Amer et al. 2016; Ghayesh & Amabili 2013). The studies about how to quantify the deviation to the exact resonance relations have been investigated systematically and analytically in references (Qian et al. 2018a; Qian et al. 2018b).

For brevity, the conclusions proposed by Qian et al. (2018a) are adopted here to quantify the deviation to the exact resonance relations. According to equation (49) in Qian et al. (2018a) and Equation (10), the transition curves which divide the resonance region and non-resonance region are obtained as

$$\omega = 2\omega_1 \pm 2\sqrt{T_{11}^2 + T_{12}^2}, \quad \omega = 2\omega_2 \pm 2\sqrt{T_{21}^2 + T_{22}^2}, \tag{16}$$

where T_{11}, T_{12}, T_{21}, T_{22} are decided by the system's parameters and can be found in the Appendix.

Based on Equation (16), the frequencies relation between the parametric frequency ω and the system's natural frequency ω_1/ω_2 can be determined, which shows the resonance region with two transition curves emanating from exact resonance relations. For example, the resonance region can be numerically determined in the $\mu - \beta$ plane for given σ and k.

4 PARAMETRIC RESONANCE ORBIT ANALYSIS

In the previous sections, we found the region in which the parametric resonance may exist by analyzing the linear part of the system in Equation (10). In the absence of the nonlinearity, when the resonance occurs, energy will be pumped into the system by parametric excitation leading to an infinite increase in the final orbit's amplitude. However, when nonlinear terms are considered, the motion will be bounded and the resonant periodic orbits can be constructed. In this section, the local nonlinear dynamics of the system are examined, and the periodic response of the system is obtained, which can further benefit the trajectory design in asteroid missions.

4.1 General Solution for Parametric Resonance Orbit

To exhibit the influence of nonlinearities, we consider the nonlinear parts of the system to the third order and omit the higher order nonlinear parametric excitation terms in Equation (6). The equation of the nonlinear motion around equilibrium points can be rewritten as

$$\begin{aligned}
\ddot{\xi} - 2\dot{\eta} - V_{\xi\xi}^0\xi - V_{\xi\eta}^0\eta =& M_1\eta^3 + M_2\xi\eta^2 + M_3\xi^2\eta + M_4\xi^3 + M_5\xi^2 + M_6\xi\eta + M_7\eta^2 \\
&+ \varepsilon^2\frac{3}{2}k\beta(\xi\cos\omega t + \eta\sin\omega t), \\
\ddot{\eta} + 2\dot{\xi} - V_{\xi\eta}^0\xi - V_{\eta\eta}^0\eta =& N_1\eta^3 + N_2\xi\eta^2 + N_3\xi^2\eta + N_4\xi^3 + N_5\xi^2 + N_6\xi\eta + N_7\eta^2 \\
&+ \varepsilon^2\frac{3}{2}k\beta(\xi\sin\omega t - \eta\cos\omega t),
\end{aligned} \tag{17}$$

where M_1, ..., M_7, N_1, ..., N_7 are nonlinear coefficients obtained by Legendre polynomial expansion of the effective potential V in Equation (8), as listed in the Appendix. The bookkeeping device ε is used to indicate the small-order parameters.

To determine the combined effect of nonlinearities and parametric excitations on the amplitude and phase, the multiple scales method is used and the solutions to Equation (17) are assumed as

$$\begin{aligned}\xi &= \varepsilon\xi_1(T_0,T_2) + \varepsilon^2\xi_2(T_0,T_2) + \varepsilon^3\xi_3(T_0,T_2),\\ \eta &= \varepsilon\eta_1(T_0,T_2) + \varepsilon^2\eta_2(T_0,T_2) + \varepsilon^3\eta_3(T_0,T_2),\end{aligned} \tag{18}$$

where $T_0 = t$ and $T_2 = \varepsilon^2 t$. Then, the time derivative becomes, $d/dt = D_0 + \varepsilon^2 D_2 + ..., D_n = \partial/\partial T_n$. Substituting Equation (18) to Equation (17), expanding, and equating coefficients of ε_1 ,ε_2 and ε_3 on both sides lead to:

$$\begin{aligned}\varepsilon^1:\quad & D_0^2\xi_1 - 2D_0\eta_1 - V^0_{\xi\xi}\xi_1 - V^0_{\xi\eta}\eta_1 = 0\\ & D_0^2\eta_1 + 2D_0\xi_1 - V^0_{\xi\eta}\xi_1 - V^0_{\eta\eta}\eta_1 = 0\end{aligned} \tag{19}$$

$$\begin{aligned}\varepsilon^2:\quad & D_0^2\xi_2 - 2D_0\eta_2 - V^0_{\xi\xi}\xi_2 - V^0_{\xi\eta}\eta_2 = M_5\xi_1^2 + M_6\xi_1\eta_1 + M_7\eta_1^2\\ & D_0^2\eta_2 + 2D_0\xi_2 - V^0_{\xi\eta}\xi_2 - V^0_{\eta\eta}\eta_2 = N_5\xi_1^2 + N_6\xi_1\eta_1 + N_7\eta_1^2\end{aligned} \tag{20}$$

$$\begin{aligned}\varepsilon^3:\quad & D_0^2\xi_3 - 2D_0\eta_3 - V^0_{\xi\xi}\xi_3 - V^0_{\xi\eta}\eta_3 = -2D_0D_2\xi_1 + 2D_2\eta_1 + \frac{3}{2}k\beta(\cos\omega t\xi_1 + \sin\omega t\eta_1)\\ &\qquad + M_1\eta_1^3 + M_2\xi_1\eta_1^2 + M_3\xi_1^2\eta_1 + M_4\xi_1^3\\ &\qquad + (2M_5\xi_1 + M_6\eta_1)\xi_2 + (M_6\xi_1 + 2M_7\eta_1)\eta_2\\ & D_0^2\eta_3 + 2D_0\xi_3 - V^0_{\xi\eta}\xi_3 - V^0_{\eta\eta}\eta_3 = -2D_0D_2\eta_1 - 2D_2\xi_1 + \frac{3}{2}k\beta(\sin\omega t\xi_1 - \cos\omega t\eta_1)\\ &\qquad + N_1\eta_1^3 + N_2\xi_1\eta_1^2 + N_3\xi_1^2\eta_1 + N_4\xi_1^3\\ &\qquad + (2N_5\xi_1 + N_6\eta_1)\xi_2 + (N_6\xi_1 + 2N_7\eta_1)\eta_2.\end{aligned} \tag{21}$$

It is easy to obtain the general solution of Equation (19) as

$$\xi_1 = A_1e^{i\omega_1T_0} + A_2e^{i\omega_2T_0} + cc, \quad \eta_1 = \Gamma_1A_1e^{i\omega_1T_0} + \Gamma_2A_2e^{i\omega_2T_0} + cc, \tag{22}$$

where cc denotes the complex conjugation of all the preceding terms of the right-hand side and

$$\Gamma_1 = \frac{-\omega_1^2 - V^0_{\xi\xi}}{2i\omega_1 + V^0_{\xi\eta}}, \quad \Gamma_2 = \frac{-\omega_2^2 - V^0_{\xi\xi}}{2i\omega_2 + V^0_{\xi\eta}}. \tag{23}$$

Note that A_1 and A_2 are considered as functions of the slow time T_2 instead of being constants as in the corresponding linear case.

Substituting ξ_1 and η_1 of Equation (22) into Equation (20), the solution to Equation (20) can be obtained. Then, substituting both ξ_1, η_1 and ξ_2, η_2 back into Equation (21) yields

$$\begin{aligned} D_0^2\xi_3 - 2D_0\eta_3 - V^0_{\xi\xi}\xi_3 - V^0_{\xi\eta}\eta_3 &= (-2i\omega_1 + 2\Gamma_1)D_2A_1e^{i\omega_1T_0} + (-2i\omega_2 + 2\Gamma_2)D_2A_2e^{i\omega_2T_0}\\ &\quad + \frac{3k\beta}{4}\bar{A}_2\left(1 - i\bar{\Gamma}_2\right)e^{i(\omega-\omega_2)T_0} + W_{11}e^{i\omega_1T_0} + W_{12}e^{i\omega_2T_0} + \ldots + cc,\\ D_0^2\eta_3 + 2D_0\xi_3 - V^0_{\xi\eta}\xi_3 - V^0_{\eta\eta}\eta_3 &= (-2i\omega_1\Gamma_1 - 2)D_2A_1e^{i\omega_2T_0} + (-2i\omega_2\Gamma_2 - 2)D_2A_2e^{i\omega_2T_0}\\ &\quad - \left(i + \bar{\Gamma}_2\right)\frac{3k\beta}{4}\bar{A}_2e^{i(\omega-\omega_2)T_0} + S_{11}e^{i\omega_1T_0} + S_{12}e^{i\omega_2T_0} + \ldots + cc,\end{aligned} \tag{24}$$

where the bar notations over A_2 and Γ_2 denote their conjugate complexes. S_{11}, S_{12}, W_{11}, W_{12} are obtained by the combination of coefficients and their expressions can be found in the Appendix.

The second-principal resonance is considered as an example in this study and the first-principal resonance can be analyzed in a similar way. A detuning parameter τ is introduced as

$$\omega = 2\omega_2 + \varepsilon^2\tau. \tag{25}$$

To determine the solvability conditions of Equation (24), we seek a particular solution of ξ_3 and η_3 corresponding to the term containing the factors $\exp(i\omega_1T_0)$ and $\exp(i\omega_2T_0)$ as

$$\xi_3 = P_1e^{i\omega_1T_0} + Q_1e^{i\omega_2T_0} + cc, \quad \eta_3 = P_2e^{i\omega_1T_0} + Q_2e^{i\omega_2T_0} + cc. \tag{26}$$

By substituting Equation (26) into Equation (24), using $(\omega - 2\omega_2)T_0 = \omega_2 T_0 + \tau T_2$ to eliminate the secular terms, and equating the coefficients of $\exp(i\omega_1 T_0)$ and $\exp(i\omega_2 T_0)$ on both sides, we

$$\begin{array}{l}\left(-\omega_1^2 - V_{\xi\xi}^0\right) P_1 + \left(-2i\omega_1 - V_{\xi\eta}^0\right) P_2 = W_1 \\ \left(2i\omega_1 - V_{\eta\xi}^0\right) P_1 + \left(-\omega_1^2 - V_{\eta\eta}^0\right) P_2 = W_2 \\ \left(-\omega_2^2 - V_{\xi\xi}^0\right) Q_1 + \left(-2i\omega_2 - V_{\xi\eta}^0\right) Q_2 = S_1 \\ \left(2i\omega_2 - V_{\eta\xi}^0\right) Q_1 + \left(-\omega_2^2 - V_{\eta\eta}^0\right) Q_2 = S_2.\end{array} \tag{27}$$

where

$$\begin{array}{l}W_1 = -2i\omega_1 D_2 A_1 + 2\Gamma_1 D_2 A_1 + W_{11}, \\ W_2 = -2i\omega_1 \Gamma_1 D_2 A_1 - 2D_2 A_1 + S_{11}, \\ S_1 = -2i\omega_2 D_2 A_2 + 2\Gamma_2 D_2 A_2 + W_{12} e^{i\tau T_2} + \left(1 - i\bar{\Gamma}_2\right) \frac{3k\beta}{4} \bar{A}_2 e^{i\tau T_2}, \\ S_2 = -2i\omega_2 \Gamma_2 D_2 A_2 - 2D_2 A_2 + S_{12} e^{i\tau T_2} - \left(i + \bar{\Gamma}_2\right) \frac{3k\beta}{4} \bar{A}_2 e^{i\tau T_2}.\end{array} \tag{28}$$

Thus, the problem of determining the solvability conditions of Equation (24) is reduced to that of determining the solvability conditions of Equation (27), which lead to

$$\begin{array}{l}D_2 A_1 = i\frac{1}{2}\Lambda_1 \left[\left(R_{21} + iI_{21}\right) A_1^2 \bar{A}_1 + \left(R_{31} + iI_{31}\right) A_1 A_2 \bar{A}_2\right], \\ D_2 A_2 = i\frac{1}{2}\Lambda_2 \left[\left(R_1 + iI_1\right) \bar{A}_2 e^{i\tau T_2} + \left(R_{22} + iI_{22}\right) A_2^2 \bar{A}_2 + \left(R_{32} + iI_{32}\right) A_1 \bar{A}_1 A_2\right],\end{array} \tag{29}$$

where

$$\Lambda_1 = \frac{\left(\omega_1^2 + V_{\eta\eta}^0\right)}{\omega_1 \left(4 - 2\omega_1^2 - V_{\xi\xi}^0 - V_{\eta\eta}^0\right)}, \quad \Lambda_2 = \frac{\left(\omega_2^2 + V_{\eta\eta}^0\right)}{\omega_2 \left(4 - 2\omega_2^2 - V_{\xi\xi}^0 - V_{\eta\eta}^0\right)}. \tag{30}$$

The coefficients $R_1, R_{21}, R_{31}, R_{22}, R_{32}, I_1, I_{21}, I_{31}, I_{22}, I_{32}$ in Equation (29), which are all functions of system's nonlinear coefficients $M_1, ..., M_7, N_1, ..., N_7$ and can be found in the Appendix, represent the system's nonlinearity.

Letting A_1 and A_2 in Equation (29) be in the polar form with real $a_n, \beta_n (n = 1, 2)$ as

$$A_1\left(T_2\right) = 0.5 a_1 e^{i\beta_1 T_2}, \quad A_2\left(T_2\right) = 0.5 a_2 e^{i\beta_2 T_2}. \tag{31}$$

Then, separating real and imaginary parts, and introducing

$$\varphi_1 = \beta_1, \quad \varphi_2 = \tau T_2 - 2\beta_2, \tag{32}$$

we have

$$\begin{array}{l}D_2 a_1 = -\Lambda_1 I_{21} \frac{a_1^3}{8} - \Lambda_1 I_{31} \frac{a_1 a_2^2}{8}, \\ a_1 D_2 \varphi_1 = \Lambda_1 R_{21} \frac{a_1^3}{8} + \Lambda_1 R_{31} \frac{a_1 a_2^2}{8}, \\ D_2 a_2 = -\Lambda_2 I_1 \frac{a_2}{2} \cos\varphi_2 - \Lambda_2 R_1 \frac{a_2}{2} \sin\varphi_2 - \Lambda_2 I_{22} \frac{a_2^3}{8} - \Lambda_2 I_{32} \frac{a_1^2 a_2}{8}, \\ a_2 D_2 \varphi_2 = a_2 \tau - \Lambda_2 R_1 a_2 \cos\varphi_2 + \Lambda_2 I_1 a_2 \sin\varphi_2 - \Lambda_2 R_{22} \frac{a_2^3}{4} - \Lambda_2 R_{32} \frac{a_1^2 a_2}{4}.\end{array} \tag{33}$$

Equation (33) can be used to ascertain the influence of the nonlinearities. In this case, the nonlinear terms involving $(R_1, R_{21}, R_{31}, R_{22}, R_{32}, I_1, I_{21}, I_{31}, I_{22}, I_{32})$ may not only affect the amplitude directly, but also affect the amplitude indirectly through changing the phase $\varphi_n (n = 1, 2)$. Therefore, we can present the first-order approximation for the general solution Equation (22) as,

$$\begin{array}{l}\xi_1 = \frac{a_1}{2} e^{i(\omega_1 T_0 + \varphi_1)} + \frac{a_2}{2} e^{i\frac{1}{2}(\omega T_0 - \varphi_2)} + cc, \\ \eta_1 = \Gamma_1 \frac{a_1}{2} e^{i(\omega T_0 + \varphi_1)} + \Gamma_2 \frac{a_2}{2} e^{i\frac{1}{2}(\omega T_0 - \varphi_2)} + cc.\end{array} \tag{34}$$

Equation (34) is quite different from the linear solution of the system. The amplitude of the linear solution can be chosen as any value. However, in Equation (34), the variations of $a_n, \varphi_n (n = 1, 2)$ strictly follow Equation (33) which involves both the transient motions and steady-state motions and a_n, φ_n are affected by the system's nonlinearity.

It is worth mentioning that, among the general solution, the steady-state motion part is periodic. It is clear that, considering the influence of nonlinear terms, the amplitudes in the resonance may no longer be unbounded. With the periodic excitation from the M_4, it is possible to find the parametric resonance orbit that will benefit the future orbit design for asteroid exploration missions.

4.2 Steady-state Motion for General Solution

According to Equation (33), when we consider the nonlinearity, the increase of amplitude is accompanied by a change in the phase $\varphi_n (n = 1, 2)$ when energy is pumped into the system by the parametric excitation. It is reasonable to consider that, when the rate at which energy is being pumped into the system is exactly balanced by the rate at which is being limited by the nonlinear effects, the system achieves a steady-station motion. Thereby, the amplitude and phase will be restricted by the nonlinearity to finite and fixed values, which means $a_1' = a_2' = 0$ and $\varphi_1' = \varphi_2' = 0$ (Nayfeh & Mook 1995).

The $a_1' = a_2' = 0$ and $\varphi_1' = \varphi_2' = 0$ correspond to the singular points of Equation (33), where the amplitude and phase do not change. Based on Equation (33), it is clear that $a_1 = 0$ must be the steady-state motion for the first modal motion (i.e., motion relevant to ω_1). Then, the steady-state motions corresponding to the solutions of the second modal motion (i.e., motion relevant to ω_2) must be

$$\begin{aligned} D_2 a_{20} = L_1 &= -\Lambda_2 I_1 \tfrac{a_{20}}{2} \cos\varphi_{20} - \Lambda_2 R_1 \tfrac{a_{20}}{2} \sin\varphi_{20} - \Lambda_2 I_{22} \tfrac{a_{20}^3}{8} = 0, \\ a_{20} D_2 \varphi_{20} = L_2 &= a_{20}\tau - \Lambda_2 R_1 a_{20} \cos\varphi_{20} - \Lambda_2 R_{22} \tfrac{a_{20}^3}{4} = 0, \end{aligned} \tag{35}$$

where the subscript 0 denotes steady-state values.

For further discussion of these results, it is more direct to rearrange $\cos\varphi_{20}$ and $\sin\varphi_{20}$, where we find either the trivial solution $a_{20} = 0$ or nontrivial solution,

$$\Lambda_2^2 \left(R_{22}^2 + I_{22}^2\right) a_{20}^4 - 8\Lambda_2 R_{22} \tau a_{20}^2 + 16\tau^2 - 16\Lambda_2^2 \left(R_1^2 + I_1^2\right) = 0. \tag{36}$$

Here we express the steady-state amplitude of the response a_{20} as a function of detuning parameter τ. Recall that Equation (36) also stands for the relation between steady-state amplitude and the frequency of parametric excitation ($\tau = \omega - 2\omega_2$) which is named as *frequency-response equation*. Once the frequency of the excitation ω and system parameters are given, the amplitude of the response a_{20} is determined.

Hence, we can present the steady-state solution as:

$$\xi_1 = \frac{a_{20}}{2} e^{i\frac{1}{2}(\omega T_0 - \varphi_{20})} + cc, \quad \eta_1 = \Gamma_2 \frac{a_{20}}{2} e^{i\frac{1}{2}(\omega T_0 - \varphi_{20})} + cc, \tag{37}$$

where φ_{20}, a_{20} are given by Equation (35) and Equation (36), respectively.

Since the steady-state motion φ_{20} is a constant, we notice in Equation (37) the nonlinearity limits the motions to finite-amplitude motions whose frequency is exactly one half the frequency of the excitation. It is a typical subharmonic resonance.

4.3 Stability of Steady-state Motion for General Solution

Based on Equation (36), we find that it is possible for one detuning parameter τ to result in two values of steady-state amplitude solution a_{20}. It is necessary to evaluate the stability of the steady-state solution since only the stable value of a_{20} can be chosen for orbit design.

Determining the stability of the steady-state solution is precisely the problem of determining the nature of singular points of Equation (35). The Jacobi matrix for Equation (35) is

$$[\mathrm{A}] = \begin{bmatrix} \frac{\partial L_1}{\partial a_{20}} & \frac{\partial L_1}{\partial \varphi_{20}} \\ \frac{\partial L_2}{\partial a_{20}} & \frac{\partial L_2}{\partial \varphi_{20}} \end{bmatrix} = \begin{bmatrix} -\frac{\Lambda_2 I_{22} a_{20}^2}{4} & \frac{\Lambda_2 R_{22} a_{20}^3 - 4\tau a_{20}}{8} \\ -\frac{\Lambda_2 R_{22} a_{20}^2}{2} & -\frac{\Lambda_2 I_{22} a_{20}^3}{4} \end{bmatrix}. \tag{38}$$

The eigenvalues of $[\mathrm{A}]$ are

$$\lambda_{1,2} = \frac{1}{2} p \pm \left(\frac{1}{4} p^2 - q\right)^{1/2}, \tag{39}$$

where p is the trace of $[\mathrm{A}]$ and q is the determinant of $[\mathrm{A}]$, and

$$p = -\frac{\Lambda_2 I_{22} \left(a_{20}^2 + a_{20}^3\right)}{4}, \quad q = \frac{\Lambda_2^2 a_{20}^5 \left(I_{22}^2 + R_{22}^2\right) - 4\tau \Lambda_2 R_{22} a_{20}^3}{16}. \tag{40}$$

Based on Equation (39), the well-known diagram of $p - q$ plane characterizing different singular points is presented in Figure 3.

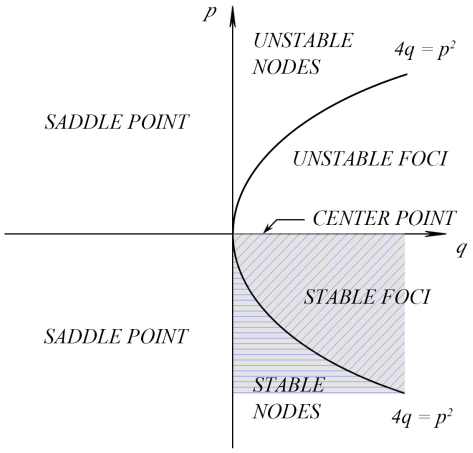

Fig. 3 Singular points in $p-q$ plane.

Thus, for Equation (35), the stable region in $p-q$ plane is shown in the shadowed area. Specially, when $p=0$, if q is positive, the singular point is a stable center point and if q is negative, the singular point is a saddle point. Equation (40) will be used to evaluate the stability of the steady-state amplitude solution a_{20} during orbit design in Section 5.

5 NUMERICAL SIMULATIONS

Numerical simulations are performed to demonstrate the designing process of such novel parametric resonance periodic orbits. The $\sigma=0.8$, $k=0.9$ are chosen as known parameters during the simulations. Firstly, the resonance region is located in the $\mu-\beta$ plane by the two preconditions presented in Section 3. Then, the frequency-response curve is obtained by Equation (36) with detailed explanations. The corresponding stability for steady-state motions is analyzed. Finally, the periodic parametric resonance orbits are found.

5.1 Parametric Resonance Region

Precondition I about the stable equilibrium point in Equation (12) and Precondition II about frequencies relations in Equation (16) are used to guarantee the existing region for parametric resonance.

The grey areas in Figure 4 indicate a threshold that satisfies Precondition I in Equation (12). The red line is the boundary of the threshold. According to the definitions for natural frequency in Equation (13) and parametric frequency in Equation (15), the blue lines denote the exact resonance relations that $\omega=2\omega_2$. We notice that the parametric amplitude and parametric frequency are all functions of β and k, and the unperturbed system's natural frequency is a function of k, β, σ, and μ. It is interesting to find that, instead of the exact resonance relation point in most mechanical systems (Remigius et al. 2019), we have the exact resonance relation lines.

In addition, as presented in Figure 4, the two black lines denote the transition boundaries from non-resonance to resonance, and the region between these two black lines represents resonance area. The deviation from the transition boundaries to the exact resonance relation line corresponds to the analytical results $\pm 2\sqrt{T_{21}^2+T_{22}^2}$ obtained from Equation (16). It is found that the larger values of β and μ lead to the larger resonance region for given σ and μ in Figure 4(a). Reminding us of that, the larger the mass parameter μ is, the more irregular the asteroid is. The larger the fourth body's characteristic parameter β is, the stronger the parametric excitation. In other words, the irregularity of the asteroid and strong gravitational influence from the fourth body play a key role to generate parametric resonance. In Figure 4(b), when $\beta=0$, the system recovers to the classical particle-linkage model, which only contains the asteroid itself and no parametric resonance occurs. When $\mu=0$, the system recovers to the regular asteroid, parametric resonance only can occur in a very small interval that $\beta\in[3.085\times 10^{-3}, 3.355\times 10^{-3}]$. Besides, with the increase of the β and μ, the lower boundary trends downward until reaching the border of the grey area obtained by Precondition I. The shaded area denotes the final valid ranges of μ, β for it to be found that parametric resonance occurs.

It is clear that, combining Precondition I and Precondition II, the final valid ranges of μ, σ, k, β for parametric resonance can be found. Any real asteroid with parameters stratifying both Precondition I and Precondition II has the potential to generate parametric resonance orbits.

5.2 Frequency-response Curves

Based on Equation (36), the response amplitude a_{20} is plotted as a function of detuning parameter τ with $k\beta=0.09$ in Figure 5. The parameters ($\sigma=0.8$, $k=0.9$, $\mu=0.001$, $\beta=0.1$) are selected from the shaded areas in Figure 4. There are two nontrivial solution branches: one stable and the other unstable. The solid lines denote the stable solutions and dashed lines denote the unstable solutions. Detailed analysis about the stability of the nontrivial solutions will be discussed in Section 5.3.

Let us suppose that τ decreases from 0.5 to -1.5. This process is represented by the black arrows through points A_1, A_2 and A_4. Correspondingly, three regions are marked as I, II and III based on different dynamic behaviors. Between points A_1 and A_2 ($\tau=0.388$), no nontrivial

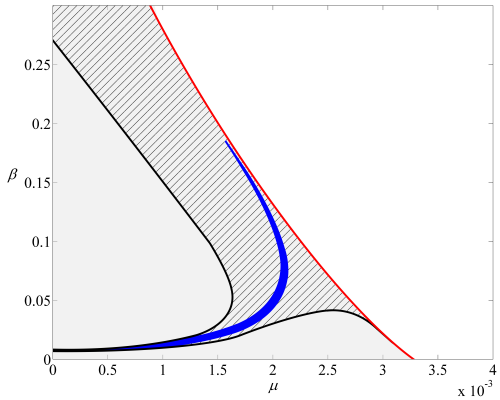

Overall view of parametric resonance region

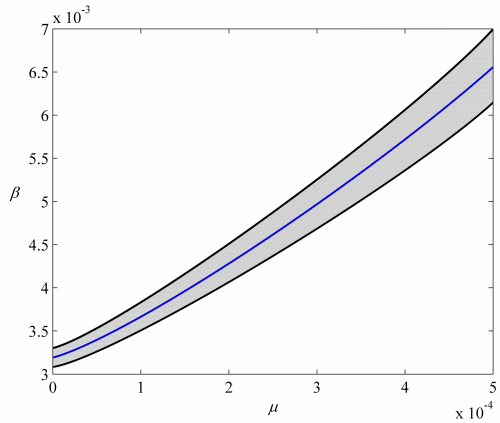

Partially enlarged view when μ and β are close to 0

Fig. 4 Parametric resonance region for the second principal resonance when $\sigma = 0.8$, $k = 0.9$.

solution exists which means that amplitude of parametric resonance orbit remains zero until point A_2. Between points A_2 and A_4 ($\tau = -0.388$), the only realizable solution is given by Equation (36). The amplitude of this solution branch increases as the frequency of excitation is decreased. Beyond point A_4, there is one trivial solution and two nontrivial solutions given by Equation (36). The results for the nonlinear system show that only the larger of the two possible nontrivial solutions are stable.

If τ increases from -1.5 to 0.5, this process is indicated by blue arrows through points A_3, A_4, A_2 and A_1. There are two nontrivial solutions exit until τ reaching point A_3. Then, the jumping phenomenon to point A_4 can be observed. Similar to the aforementioned τ decreasing process, from A_4 to A_2, the only realizable solution is given by Equation (36). Between points A_2 and A_1, no nontrivial solution exists.

In region I, it appears that the responses to all initial disturbances, regardless of how large the amplitude, decay in region I. Based on Equation (33), we note that the nonlinearity can affect the amplitude indirectly through changing the phase. Thus we conclude that, for the nonlinear system, in this region, the phasing is such that the force actually does negative work and thus contributes to the decaying behavior.

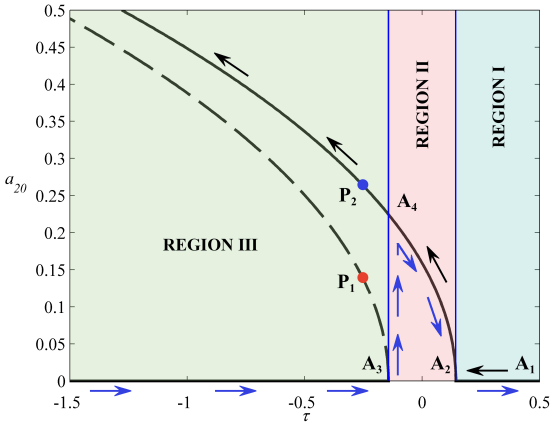

Frequency-amplitude response curves

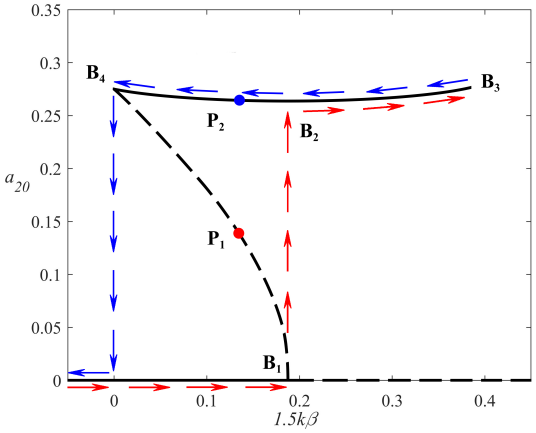

Amplitude of the excitation-amplitude of response curves

Fig. 5 Response curves for the asteroid's parametrically excited system

The behaviors of the solutions in region II and III are certainly dependent on the nonlinearity. In region II, the response of the nonlinear system is a bounded limit cycle. Thus in region II, all initial disturbances trigger the same steady-state response.

In region III, the response of the nonlinear system may either decay (trivial solution) or achieve a sustained periodic motion (nontrivial solution). It appears that for some initial disturbances, the nonlinear term does not have a strong influence on the resulting motion and the system behaves essentially as a linear system; the motion decays. On the other hand, for other initial disturbances the nonlinear term has a strong influence; phase changes

such as those described for region II occur, and a nontrivial steady-state solution exists. Thus, in region III, there is the possibility of producing motions that have characteristics that are similar to those of the motions in region I as well as region II. The initial conditions determine which steady-state solution is physically realizable by the system.

In Figure 5(b), a_{20} is plotted as a function of amplitude of the excitation $1.5k\beta$ with constant detuning parameter τ = -0.2548. With the increase of $k\beta$, the process is shown by red arrows. The a_{20} remains zero until B_1, and then jumps to B_2. Further increase of the $k\beta$ causes the a_{20} to follow the red arrows to B3. When the $k\beta$ decreases, the process is shown by blue arrows. The a_{20} follows the curve through B_3, B_2 to B_4. Further decrease of the $k\beta$ cause the a_{20} jumps to zero.

5.3 Stability of Steady-state Motion Amplitude and Periodic Parametric Resonance Orbit

Based on Equation (25), when $\sigma = 0.8$, $k = 0.9$, $\mu = 0.001$, $\beta = 0.1$, the detuning parameter is obtained as $\tau = -0.2548$. There are two nontrivial solutions for the steady-state motion amplitude, $a_{20} = 0.2646$ and $a_{20} = 0.1399$ according to Equation (36) which are marked as P_2 and P_1 in Figure 5.

Equation (40) is used to evaluate the stability of the nontrivial solutions. Since p and q are all functions of a_{20}, τ and nonlinear coefficients, it is to find the values, $p = 0, q = 0.0151$ for $a_{20} = 0.2646$ and $p = 0, q = -0.0022$ when $a_{20} = 0.1399$. As we concluded in Section 4.3, when $p = 0$ and q is positive, the corresponding value of state-state amplitude is stable and if q is negative, the corresponding value of state-state amplitude is unstable. Thus, we conclude that $a_{20} = 0.2646$ is a stable solution for steady-state motion amplitude and $a_{20} = 0.1399$ is an unstable solution. Since there are no damping terms considered in the system, the singular points of the system must not be a node or a focus.

To illustrate these results further, we used Equation (35) to calculate several trajectories in the state flow chart in $a_{20} - \varphi_{20}$ plane for values of amplitude of the excitation a_{20} and detuning parameter τ falling in region II of Figure 5(a). These trajectories are plotted in Figure 6(a). The saddle point ($a_{20} = 0.1399, \varphi_{20} = 0$) corresponds to the unstable, nontrivial steady-state solution, which is the exact value of P_1 in Figure 5(a) and Figure 5(b). Similarly, center point P_2 ($a_{20} = 0.2646, \varphi_{20} = \pi$) corresponds to the stable, nontrivial steady-state solution when more than one steady-state solution exists. These points correspond to those labeled in Figure 5(a) and Figure 5(b). All initial conditions in the shaded area lead to nontrivial solution.

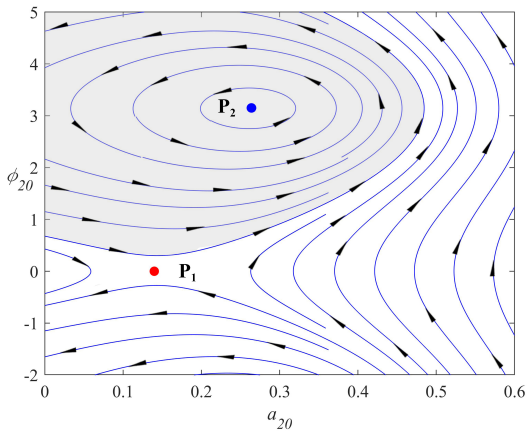

$\sigma = 0.8, k = 0.9, \mu = 0.001, \beta = 0.1$

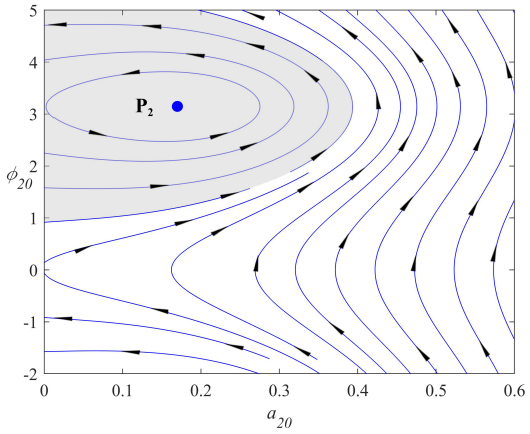

$\sigma = 0.8, k = 0.9, \mu = 0.0019, \beta = 0.1$

Fig. 6 State flow chart.

The arrows indicate the direction of the motion of the representative point. The initial conditions determine which one is reached.

Similarly, we slightly adjust the value of μ into 0.0019 and keep the values of the rest parameters. The corresponding detuning parameter is obtained as $\tau = -0.2548$. There is only one nontrivial solution for the steady-state motion amplitude, $a_{20} = 0.17043$ according to Equation (36). Equation (40) is used to evaluate its stability. It is found that, when $a_{20} = 0.17043$, $p = 0$, $q = 0.02209$, and this nontrivial solution is stable. The state flow chart in $a_{20} - \varphi_{20}$ plane for values of amplitude of the excitation and frequency is also plotted in Figure 6(b). The center point P_2 ($a_{20} = 0.17043, \varphi_{20} = \pi$) corresponds to the stable, nontrivial steady-state solution. The arrows indicate the direction of the motion of the representative point. All initial conditions in the shaded area lead to nontrivial solutions.

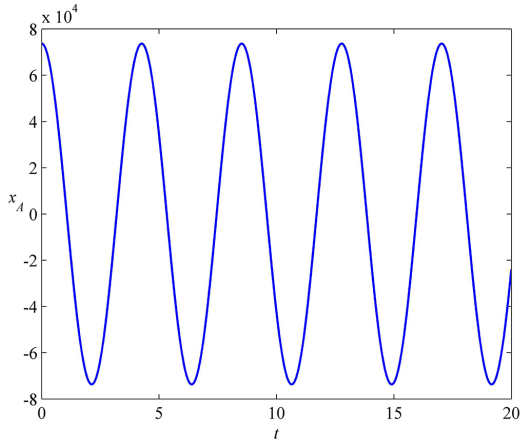

Time history diagram for fourth primary's x-motion

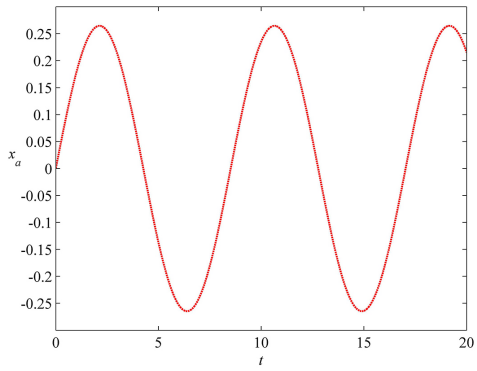

Time history diagram for parametric resonance x-motion

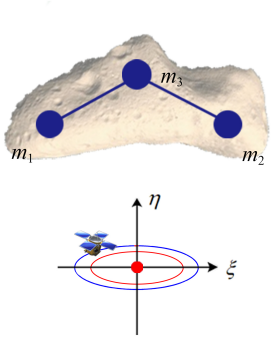

Actual parametric resonance trajectory in $L_0 - \xi\eta$ coordinate system

Fig. 7 Periodic stable parametric resonance orbit when $\sigma = 0.8$, $k = 0.9$, $\mu = 0.001$, $\beta = 0.1$

With the stable solution for the state-state amplitude a_{20} and phase φ_{20}, we present a possible periodic orbit that can be utilized as nominal orbits for practical space missions. Based on Equation (37), we plot both periodic motions for the fourth primary and the parametric resonance orbit to show the synthesis of these two types of periodic motions in Figure 7(a)−7(b) when $\sigma = 0.8$, $k = 0.9$, $\mu = 0.001$, $\beta = 0.1$. It is clear that the nonlinearity of the system plays a major role in adjusting the frequency of the parametric resonance to exactly one half the frequency of the excitation. When $\sigma = 0.8$, $k = 0.9$, $\mu = 0.0019$, $\beta = 0.1$, the actual trajectory is shown in red in Figure 7(c). It should be noted that the spacecraft's trajectory is shown in the $L_0 - \xi\eta$ coordinate system. The origin of this coordinate denoted by red point is the stable equilibrium point L_4 of the asteroid, which is determined by Equation (12).

Although the final trajectory for the steady-state motion shows up as an ellipse that looks like Lyapunov orbit, it actually comes from a totally different family of orbits. The frequency of the parametric resonance orbit is decided by the frequency of the excitation while the natural frequency of the Lyapunov orbit is decided by the system's characteristic equation without consideration of the periodic excitation of the fourth primary.

It is worth mentioning that μ, σ, k, β are parameters for the perturbed asteroid system itself and β is the parameter about the Sun's gradational perturbation. One group of μ, σ, k, β that satisfies Preconditions I and II can only result in one first principal parametric resonance orbit or one second principal parametric resonance orbit. The conditions to generate parametric resonance orbits are critical, and not all of the asteroid systems are qualified.

In this study, we used a hypothetical asteroid system in simulations. Since the conditions to generate parametric resonance orbits are critical, no already-found asteroids undergo such parametric resonance, although some unknown parametric resonance asteroids may be found in the future.

6 CONCLUSIONS

Based on the idea of integrating the solar gradational force as part of the system instead of treating it as perturbations, the concept of parametric resonance from nonlinear oscillation theory is adopted to design a novel type of parametric resonance orbits for irregular asteroids.

The resonance region is located in μ (mass parameter)-β (fourth body's characteristic parameter) plane. It is found that the irregularity of the asteroid and gravitational influence from the fourth body are important in generating parametric resonance, and larger values of β and μ lead to larger resonance region.

The frequency-response curves are obtained and explained in detail. Based on the number of non-trivial solutions, three regions are classified in the plane of steady-state amplitude a_{20} and detuning parameter τ. The stability for steady-state motions is analyzed. During the process of increasing τ, the jumping phenomenon can be observed.

With the stable solution for the state-state amplitude and phase, we introduced the stable periodic orbits caused by parametric resonance. It is clear that the nonlinearity of the system plays a major role in adjusting the frequency of the parametric resonance to exactly one half of the frequency of the excitation. This study expands a set of existing periodic solutions for the asteroid system.

In addition, since the asteroid is considered as a few primaries separated by massless rods by the particle-linkage model, the proposed method about the parametric resonance orbit for irregular asteroids can also be used to understand the dynamical behaviors parametric resonance orbits for the binary and triple asteroids system.

Acknowledgements This work was supported in part by the National Natural Science Foundation of China (Project Nos. 11772009, 11972007 and 11832002), the Beijing Municipal Natural Science Foundation (Project No. 1192002), and the International Research Cooperation Seed Fund of Beijing University of Technology (No. 2018B15).

APPENDIX

$$
\begin{aligned}
&T_{w1}=\frac{H_{w1}H_{w3}+H_{w2}H_{w4}}{H_{w1}^2+H_{w2}^2}, T_{w2}=\frac{H_{w1}H_{w4}-H_{w2}H_{w3}}{H_{w1}^2+H_{w2}^2}, w=1,2\\
&H_{w1}=2\left(\omega_w^2+V_{\xi\xi}^0\right)\left(1-\omega_w\rho_{w2}\right)-4\omega_w^2+4\omega_w\rho_{w2}+2V_{\xi_7}^0\rho_{w1}\\
&H_{w2}=2\left(\omega_w^2+V_{\xi\xi}^0\right)\rho_{w1}\omega_w-4\rho_{w1}\omega_w+2V_{\xi\eta}^0\left(\rho_{w2}-\omega_w\right)\\
&H_{w3}=\frac{3}{4}k\beta\left(\omega_w^2+V_{\xi\xi}^0\right)\rho_{w1}-\frac{3}{2}k\beta\rho_{w1}\omega_w+\frac{3}{4}k\beta V_{\xi\eta}^0\left(1-\rho_{w2}\right)\\
&H_{w4}=\frac{3}{4}k\beta\left(\omega_w^2+V_{\xi\xi}^0\right)\left(1-\rho_{w2}\right)-\frac{3}{2}k\beta\omega_w\left(1-\rho_{w2}\right)-\frac{3}{4}k\beta V_{\xi\eta}^0\rho_{w1}\\
&\rho_{w1}=\frac{-V_{\xi\eta}^0\left(\omega_w^2+V_{\xi\xi}^0\right)}{4\omega_w^2+\left(V_{\xi\eta}^0\right)^2}, \rho_{w2}=\frac{2\omega_w\left(\omega_w^2+V_{\xi\xi}^0\right)}{4\omega_w^2+\left(V_{\xi\eta}^0\right)^2}
\end{aligned}
$$

$$
\begin{aligned}
W_{11}=&3\Gamma_1^2\bar{\Gamma}_1A_1^2\bar{A}_1M_1+6\Gamma_1\Gamma_2\bar{\Gamma}_1A_1A_2\bar{A}_2M_1+3A_1^2\bar{A}_1M_4+6A_1A_2\bar{A}_2M_4\\
&+2\Gamma_1\Gamma_2A_1A_2\bar{A}_2M_2+2\Gamma_1\bar{\Gamma}_2A_1A_2\bar{A}_2M_2+2\Gamma_1\bar{\Gamma}_1A_1^2\bar{A}_1M_2\\
&+2\Gamma_2\bar{\Gamma}_2A_1A_2\bar{A}_2M_2+\Gamma_1^2A_1^2\bar{A}_1M_2+2\bar{\Gamma}_2A_1A_2\bar{A}_2M_3+2\Gamma_2A_1A_2\bar{A}_2M_3\\
&+2\Gamma_1A_1^2\bar{A}_1M_3+2\Gamma_1A_1A_2\bar{A}_2M_3+\bar{\Gamma}_1A_1^2\bar{A}_1M_3\\
W_{12}=&3\Gamma_1^2\bar{\Gamma}_1A_1^2\bar{A}_1N_4+6\Gamma_1\Gamma_2\bar{\Gamma}_1A_1A_2\bar{A}_2N_4+3A_1^2\bar{A}_1N_1+6A_1A_2\bar{A}_2N_1\\
&+2\Gamma_1\Gamma_2A_1A_2\bar{A}_2N_3+2\Gamma_1\bar{\Gamma}_2A_1A_2\bar{A}_2N_3+2\Gamma_1\bar{\Gamma}_1A_1^2\bar{A}_1N_3\\
&+2\Gamma_2\bar{\Gamma}_2A_1A_2\bar{A}_2N_3+\Gamma_1^2A_1^2\bar{A}_1N_3+2\bar{\Gamma}_2A_1A_2\bar{A}_2N_2+2\Gamma_2A_1A_2\bar{A}_2N_2\\
&+2\Gamma_1A_1^2\bar{A}_1N_2+2\Gamma_1A_1A_2\bar{A}_2N_2+\bar{\Gamma}_1A_1^2\bar{A}_1N_2
\end{aligned}
$$

$$
\begin{aligned}
S_{11}=&3\Gamma_2^2\bar{\Gamma}_2A_2^2\bar{A}_2M_1+6\Gamma_1\bar{\Gamma}_1\Gamma_2A_1\bar{A}_1A_2M_1+3A_2^2\bar{A}_2M_4+6A_1\bar{A}_1A_2M_4\\
&+2\Gamma_1\Gamma_2A_1\bar{A}_1A_2M_2+2\Gamma_1\bar{\Gamma}_1A_1\bar{A}_1A_2M_2+2\Gamma_2\bar{\Gamma}_2A_2^2\bar{A}_2M_2\\
&+2\bar{\Gamma}_1\Gamma_2A_1\bar{A}_1A_2M_2+\Gamma_2\Gamma_2A_2^2\bar{A}_2M_2+2\bar{\Gamma}_1A_1\bar{A}_1A_2M_3+2\Gamma_2A_1\bar{A}_1A_2M_3\\
&+2\Gamma_2A_2^2\bar{A}_2M_3+2\Gamma_1A_1\bar{A}_1A_2M_3+\bar{\Gamma}_2A_2^2\bar{A}_2M_3\\
S_{12}=&3\Gamma_2^2\bar{\Gamma}_2A_2^2\bar{A}_2N_4+6\Gamma_1\bar{\Gamma}_1\Gamma_2A_1\bar{A}_1A_2N_4+3A_2^2\bar{A}_2N_1+6A_1\bar{A}_1A_2N_1\\
&+2\Gamma_1\Gamma_2A_1\bar{A}_1A_2N_3+2\Gamma_1\bar{\Gamma}_1A_1\bar{A}_1A_2N_3+2\Gamma_2\bar{\Gamma}_2A_2^2\bar{A}_2N_3\\
&+2\bar{\Gamma}_1\Gamma_2A_1\bar{A}_1A_2N_3+\Gamma_2\Gamma_2A_2^2\bar{A}_2N_3+2\bar{\Gamma}_1A_1\bar{A}_1A_2N_2+2\Gamma_2A_1\bar{A}_1A_2N_2\\
&+2\Gamma_2A_2^2\bar{A}_2N_2+2\Gamma_1A_1\bar{A}_1A_2N_2+\bar{\Gamma}_2A_2^2\bar{A}_2N_2
\end{aligned}
$$

$$
\begin{aligned}
R_1 + iI_1 &= \frac{3k\beta\left(1 - 2\bar{\Gamma}_2 i - \bar{\Gamma}_2^2\right)}{4} \\
R_{21} + iI_{21} &= 3M_1\Gamma_1^2\bar{\Gamma}_1 + M_2\Gamma_1^2 + 2M_2\Gamma_1\bar{\Gamma}_1 + 2M_3\Gamma_1 + M_3\bar{\Gamma}_1 + 3M_4 \\
&\quad + 3N_1\Gamma_1^2\bar{\Gamma}_1^2 + N_2\Gamma_1^2\bar{\Gamma}_1 + 2N_2\Gamma_1\bar{\Gamma}_1^2 + 2N_3\Gamma_1\bar{\Gamma}_1 + N_3\bar{\Gamma}_1^2 + 3N_4\bar{\Gamma}_1 \\
R_{31} + iI_{31} &= 6M_1\Gamma_1\Gamma_2\bar{\Gamma}_2 + 2M_2\Gamma_1\Gamma_2 + 2M_2\Gamma_1\bar{\Gamma}_2 + 2M_2\Gamma_2\bar{\Gamma}_2 \\
&\quad + 2M_3\Gamma_1 + 2M_3\Gamma_2 + 2M_3\bar{\Gamma}_2 + 6M_4 \\
&\quad + 6N_1\Gamma_1\bar{\Gamma}_1\Gamma_2\bar{\Gamma}_2 + 2N_2\Gamma_1\bar{\Gamma}_1\Gamma_2 + 2N_2\Gamma_1\bar{\Gamma}_1\bar{\Gamma}_2 + 2N_2\bar{\Gamma}_1\Gamma_2\bar{\Gamma}_2 \\
&\quad + 2N_3\Gamma_1\bar{\Gamma}_1 + 2N_3\bar{\Gamma}_1\Gamma_2 + 2N_3\bar{\Gamma}_1\bar{\Gamma}_2 + 6N_4\bar{\Gamma}_1 \\
R_{22} + iI_{22} &= 3M_1\Gamma_2^2\bar{\Gamma}_2 + M_2\Gamma_2^2 + 2M_2\Gamma_2\bar{\Gamma}_2 + 2M_3\Gamma_2 + M_3\bar{\Gamma}_2 + 3M_4 \\
&\quad + 3N_1\Gamma_2^2\bar{\Gamma}_2^2 + N_2\Gamma_2^2\bar{\Gamma}_2 + 2N_2\Gamma_2\bar{\Gamma}_2^2 + 2N_3\Gamma_2\bar{\Gamma}_2 + N_3\bar{\Gamma}_2^2 + 3N_4\bar{\Gamma}_2 \\
R_{32} + iI_{32} &= 6M_1\Gamma_1\bar{\Gamma}_1\Gamma_2 + 2M_2\Gamma_1\Gamma_2 + 2M_2\bar{\Gamma}_1\Gamma_2 + 2M_2\Gamma_1\bar{\Gamma}_1 \\
&\quad + 2M_3\Gamma_2 + 2M_3\Gamma_1 + 2M_3\bar{\Gamma}_1 + 6M_4 \\
&\quad + 6N_1\Gamma_1\bar{\Gamma}_1\Gamma_2\bar{\Gamma}_2 + 2N_2\Gamma_1\Gamma_2\bar{\Gamma}_2 + 2N_2\bar{\Gamma}_1\Gamma_2\bar{\Gamma}_2 + 2N_2\Gamma_1\bar{\Gamma}_1\bar{\Gamma}_2 \\
&\quad + 2N_3\Gamma_2\bar{\Gamma}_2 + 2N_3\Gamma_1\bar{\Gamma}_2 + 2N_3\bar{\Gamma}_1\bar{\Gamma}_2 + 6N_4\bar{\Gamma}_2
\end{aligned}
$$

$$
M_1 = \sum_{i=1}^{3} \frac{\mu_i k\left(35E_iF_i^3 - 15E_iF_iD_i^2\right)}{2\gamma_o^3 D_i^9}, \quad M_2 = \sum_{i=1}^{3} \frac{\mu_i k\left(105E_i^2F_i^2 - 15E_i^2D_i^2 - 15F_i^2D_i^2 + 3D_i^4\right)}{2\gamma_o^3 D_i^9}
$$

$$
M_3 = \sum_{i=1}^{3} \frac{\mu_i k\left(105E_i^3F_i - 45E_iF_iD_i^2\right)}{2\gamma_o^3 D_i^9}, \quad M_4 = \sum_{i=1}^{3} \frac{\mu_i k\left(35E_i^4 - 30E_i^2D_i^2 + 3D_i^4\right)}{2\gamma_o^3 D_i^9}
$$

$$
M_5 = \sum_{i=1}^{3} \frac{\mu_i k\left(15E_i^3 - 9E_iD_i^2\right)}{2\gamma_o^3 D_i^7}, \quad M_6 = \sum_{i=1}^{3} \frac{\mu_i k\left(15E_i^2F_i - 3F_iD_i^2\right)}{\gamma_o^3 D_i^7}
$$

$$
M_7 = \sum_{i=1}^{3} \frac{\mu_i k\left(15E_iF_i^2 - 3E_iD_i^2\right)}{2\gamma_o^3 D_i^7}, \quad N_1 = \sum_{i=1}^{3} \frac{\mu_i k\left(35F_i^4 - 30F_i^2D_i^2 + 3D_i^4\right)}{2\gamma_o^3 D_i^9}
$$

$$
N_2 = \sum_{i=1}^{3} \frac{\mu_i k\left(105E_iF_i^3 - 45E_iF_iD_i^2\right)}{2\gamma_o^3 D_i^9}, \quad N_3 = \sum_{i=1}^{3} \frac{\mu_i k\left(105E_i^2F_i^2 - 15F_i^2D_i^2 - 15E_i^2D_i^2 + 3D_i^4\right)}{2\gamma_o^3 D_i^9}
$$

$$
N_4 = \sum_{i=1}^{3} \frac{\mu_i k\left(35E_i^3F_i - 15E_iF_iD_i^2\right)}{2\gamma_o^3 D_i^9}, \quad N_5 = \sum_{i=1}^{3} \frac{\mu_i k\left(15E_i^2F_i - 3F_iD_i^2\right)}{2\gamma_o^3 D_i^7}
$$

$$
N_6 = \sum_{i=1}^{3} \frac{\mu_i k\left(15E_iF_i^2 - 3E_iD_i^2\right)}{\gamma_o^3 D_i^7}, \quad N_7 = \sum_{i=1}^{3} \frac{\mu_i k\left(15F_i^3 - 9F_iD_i^2\right)}{2\gamma_o^3 D_i^7}
$$

References

Alfriend, K. T., & Rand, R. H. 1968, Journal of the Astronautical Sciences, 15, 105

Amer, Y. A., El-Sayed, A. T., & Kotb, A. A. 2016, Nonlinear Dynamics, 85, 2497

Bartczak, P., & Breiter, S. 2003, Celestial Mechanics and Dynamical Astronomy, 86, 131

Bellerose, J., & Scheeres, D. J. 2007, Acta Astronautica, 60, 141

Chanut, T. G. G., Winter, O. C., & Tsuchida, M. 2014, MNRAS, 438, 2672

Eros, A., & Elipe, A. 2004, Journal of the Astronautical Sciences, 51, 391

Feng, J., & Hou, X. Y. 2019, Communications in Nonlinear Science and Numerical Simulations, 76, 71

Ghayesh, M. H., & Amabili, M. 2013, Mechanics Based Design of Structures & Machines, 41, 359

Hou, X., Xin, X., & Feng, J. 2018, Communications in Nonlinear Science and Numerical Simulations, 56, 93

Hsu, C. S. 1974, Journal of Applied Mechanics, 41, 1135

Huang, J., Ji, J., Ye, P., et al. 2013, Scientific Reports, 3, 3411

Jafari Nadoushan, M., & Assadian, N. 2015, Nonlinear Dynamics September 2015, 81, 2031

Jiang, Y., & Baoyin, H. 2016, AJ, 152, 137

Jiang, Y., Baoyin, H., & Li, H. 2015a, MNRAS, 452, 3924

Jiang, Y., Baoyin, H., Wang, X., et al. 2015b, Nonlinear Dynamics, 83, 231
Jiang, Y., Yu, Y., & Baoyin, H. 2015c, Nonlinear Dynamics, 81, 119
Jiang, Y., Schmidt, J., Li, H., Liu, X., & Yang, Y. 2017, Astrodynamics, 2, 69
Lauretta, D. S., Dellagiustina, D. N., Bennett, C. A., et al. 2019, Nature, 568, 55
Lei, H., Circi, C., & Ortore, E. 2019, MNRAS, 485, 2731
Lei, H., & Xu, B. 2015, Communications in Nonlinear Science and Numerical Simulation, 29, 441
Li, X., Qiao, D., & Barucci, M. A. 2018, Astrodynamics, 2, 133
Liu, X., Baoyin, H., Georgakarakos, N., Donnison, J. R., & Ma, X. 2012, MNRAS, 427, 1034
Mandelstam, L. 1934, Zhurnal Teknicheskoy Fiziki, 4, 67
Nardi, L., Palomba, E., Longobardo, A., Galiano, A., & Dirri, F. 2019, Icarus,, 321, 14
Nayfeh, A. H., & Mook, D. T. 1995, Nonlinear Oscillations, Wiley Classics Library (Weinheim: Wiley-VCH)
Prockter, L., Murchie, S., Cheng, A., et al. 2002, Acta Astronautica, 51, 491
Qian, Y.-J., Yang, L.-Y., Yan, X.-D., & Zhang, W. 2018a, Astrodynamics, 2, 147
Qian, Y. J., Yang, X. D., Wu, H., Zhang, W., & Yang, T. Z. 2018b, Acta Mechanica Sinica, 34, 963
Remigius, W. D., Gupta, S., & Sarkar, S. 2019, Nonlinear Dynamics, 96, 2257
Scheeres, D. J. 2012, Acta Astronautica, 72, 1
Scheeres, D. J., Ostro, S. J., Hudson, R. S., & Werner, R. A. 1996, Icarus,, 121, 67
Scheeres, D. J., Williams, B. G., & Miller, J. K. 2000, Journal of Guidance Control Dynamics, 23, 466
Shi, Y., Wang, Y., & Xu, S. 2018, Acta Astronautica, 152, 208
Shi, Y., Wang, Y., & Xu, S. 2019, Acta Astronautica, 163, 11
Wang, Y., & Xu, S. 2013, Acta Astronautica, 84, 99
Wang, Y., & Xu, S. 2014, Nonlinear Dynamics, 78, 1
Yang, H.-W., Li, S., & Xu, C. 2018, RAA (Research in Astronomy and Astrophysics), 18, 084
Yu, Y., & Baoyin, H. 2012, MNRAS, 427, 872
Zeng, X., & Alfriend, K. T. 2017, Astrodynamics, 1, 41
Zeng, X., Baoyin, H., & Li, J. 2016, Ap&SS, 361, 14
Zeng, X., Zhang, Y., Yu, Y., & Liu, X. 2018, AJ, 155, 85